Evaluation of Radiomic Features Stability When Deformable Image Registration Is Applied

Kuei-Ting Chou[1], Kujtim Latifi[2], Eduardo G. Moros[2], Vladimir Feygelman[2], Tzung-Chi Huang[1], Thomas J. Dilling[2], Bradford Perez[2] and Geoffrey G. Zhang[2,*]

[1]*Department of Biomedical Imaging and Radiological Science, China Medical University, Taichung, Taiwan*

[2]*Radiation Oncology, Moffitt Cancer Center, Tampa, FL, U.S.A.*

Keywords: Radiomic Features, Deformable Image Registration, Stability.

Abstract: Radiomic features are currently being evaluated as potential imaging biomarkers. Deformable image registration (DIR) is now routinely applied in many medical imaging applications. Usually, DIR is applied in one of two ways: a) mapping the surface of a contoured volume, or b) mapping the image intensities. This study investigated radiomic feature stability when DIR is applied in these two ways using four dimensional computed tomography (4DCT) data. DIR was applied between the inspiration and expiration phases of 4DCT datasets. Radiomic features were extracted from (1) the expiration phases of 25 lung cancer 4DCT datasets within the contoured tumor volumes, (2) the inspiration phases with the mapped tumor volumes, and (3) the inspiration phases deformed to the corresponding expiration phases of the original contoured volumes. The mean variation and the concordance correlation coefficient (CCC) between these 3 sets of features were analyzed. Many features were found unstable (mean variation > 50% or CCC < 0.5) when DIR was applied in either way. Caution is needed in radiomic feature applications when DIR is necessary.

1 INTRODUCTION

Medical images play important roles in cancer diagnosis, radiation treatment planning, and outcome evaluation. Recently, an image analysis field, known as radiomics, gained focus in the hopes of obtaining more clinically useful information from medical images. Radiomic features are quantitative values extracted from the digital images, and show potential as imaging biomarkers (Fave et al., 2017, Nardone et al., 2016). The feature values are usually calculated within a region of interest (ROI) in a 3-dimentional (3D) image set. One of the most important ROIs in radiation therapy is the gross tumor volume (GTV).

The feature extraction concept was recently expanded to images acquired at different times, for treatment response evaluation and outcome analysis (Antunes et al., 2016, Cunliffe et al., 2015, Yip et al., 2016). Image registration, most often deformable, is by definition required to properly align two separate datasets for comparison. Deformable image registration (DIR) has matured and is now a staple in radiotherapy, including, but not limited to, adaptive treatment planning (Gao et al., 2006) and pulmonary ventilation calculations (Huang et al., 2013). In the radiomics realm, when two datasets are being compared, the features can be extracted following either just the deformed contour propagation or full image deformation. For example, deformed and aligned images were used to extract features for early evaluation of renal cell carcinoma treatments (Antunes et al., 2016), and propagated contours were employed in feature extraction for lung and esophagus cancer treatment outcome predictions (Yip et al., 2016, Cunliffe et al., 2015).

At the same time, it is important to understand the limitations of radiomic features before they are used clinically. Multiple studies have attempted to elucidate the behavior of radiomic features under different conditions. Many factors can potentially affect the features' values, including image quality (Oliver et al., 2017), voxel size (Shafiq-ul-Hassan et al., 2017), motion (Carles et al., 2017, Oliver et al., 2015), segmentation (Balagurunathan et al., 2014), or acquisition and reconstruction parameters (Galavis et al., 2010), to name a few. When DIR is involved as an extra step in radiomic feature extraction, it begs a simple question: does DIR affect the feature values, and if so by how much?

Chou, K-T., Latifi, K., Moros, E., Feygelman, V., Huang, T-C., Dilling, T., Perez, B. and Zhang, G.
Evaluation of Radiomic Features Stability When Deformable Image Registration Is Applied.
DOI: 10.5220/0006694301530158
In *Proceedings of the 11th International Joint Conference on Biomedical Engineering Systems and Technologies (BIOSTEC 2018) - Volume 2: BIOIMAGING*, pages 153-158
ISBN: 978-989-758-278-3

Feature stability after image registration was evaluated by Cunliffe et al., (2012) using propagated contours. They evaluated the accuracy of features with different registration methods, including rigid, affine and deformable, and concluded that DIR gave the most accurate values. That study contributed to our understanding of DIR's effect on image features. However, the feature stability when the deformed pixel values are used, rather than just the propagated ROI masks, was not addressed. Also the number of features in that work was relatively small (140).

The objective of our study was to analyze and compare feature stability between the two DIR approaches for more than 1000 radiomic features.

2 MATERIALS AND METHODS

2.1 Image Data

Twenty-five randomly selected lung cancer cases were studied retrospectively. In each case, the end-inspiration and end-expiration phases from a 10-phase 4-dimensional CT (4DCT) dataset were used. 4DCT scans followed a standard clinical protocol, hence the voxel size, kVp and mAs settings were kept constant. All CT numbers were converted to positive values, with air corresponding to 0 and soft tissue to ~1000. The lung GTVs were manually segmented (contoured) on the end-expiration phase by an oncologist. The median contoured GTV was 6.5 cm^3, ranging between 0.8 and 46.5 cm^3.

2.2 Deformable Image Registration

Based on previous evaluations (Latifi et al., 2013b, Latifi et al., 2013a), the diffeomorphic morphons (DM) DIR algorithm (Janssens et al., 2011, Wrangsjö et al., 2005) was selected for this study because of its relatively high registration accuracy in the thoracic region. The DIR program was implemented in MatLab (The MathWorks, Natick, MA, USA) with an iterative and multiscale scheme. Eight scales were used for each registration, with up to 20 iterations at each one. A deformation matrix obtained in the registration process was applied to deform and align the images and map the contoured tumor volume from one dataset to another. Both the original and propagated contoured volumes were used as masks to extract features from the corresponding image datasets. Linear interpolation was applied when volume expansion or compression occurred.

2.3 Feature Extraction

An in-house program implemented on a PC (Oliver et al., 2015, Shafiq-ul-Hassan et al., 2017) extracted image features from inside the contoured volumes. The feature categories were shape, intensity, textural (based on the gray level co-occurrence matrix (GLCM) (Haralick et al., 1973, Liang, 2012), the gray-level size zone matrix (GLSZM) (Thibault et al., 2009), the run-length matrix (RLM) (Galloway, 1975, Chu et al., 1990), the neighborhood gray-tone difference matrix (NGTDM) (Amadasun and King, 1989)), fractal dimension (FD) (Sarkar and Chaudhuri, 1992, Jin et al., 1995), Laplacian of Gaussian (LoG) (Chen et al., 1987), wavelets (Uytterhoeven et al., 1997), and Laws (Suzuki and Yaginuma, 2007), for a grand total of 1007 features. The shape-based features included short axis (through center of mass, COM), long axes through COM and free, sphericity, eccentricity, convexity, etc. As many features were volume and/or gray level dependent (Shafiq-ul-Hassan et al., 2017), volume normalized features (Vnorm) as well as gray level normalized features (Gnorm) were also extracted.

Originally, some of the features were based on 2D images. However, the in-house program was implemented to extract all features in 3D. The feature calculations on the transformed, or filtered, images (e.g., LoG, wavelets, Laws) were performed according to Ref. (Aerts et al., 2014). LoG features were extracted with various Gaussian kernel widths. The kernel width used in this study varied from 0.5 to 3 mm with a step size of 0.5 mm. Discrete wavelet transform was applied to the original images and the wavelet features (intensity-based), were extracted from the filtered images. The combination of low pass (L) and high pass (H) filters in 3 directions generated 8 sub-categories of features. For Laws features, combination of Local (L), Edge (E) and Spot (S) convolution kernels were applied to 3D datasets before extracting the intensity features. For the Laws features, the combination of 3 kernels in 3D generated 27 sub-categories of features.

To evaluate the stability of the two possible extraction approaches (e.g., image registration vs. mapped contours), the GTV contour was mapped from the expiration to inspiration phase (Ctr_{map} in Fig.1) and the inspiration phase image was deformed to align with the expiration phase (Img_{def}). The feature values extracted from inside the ROI volume on the expiration phase ($Feature_{orig}$) were set as standards, as both the image set and the contoured volume were the originals. The feature values extracted from the data sets after the DIR

($Feature_{DIR}$), which included the mapped volume on the inspiration phase ($Feature_{vol}$) and the features from the original contoured volume on the deformed inspiration phase aligned with the expiration phase ($Feature_{img}$), were compared to the standard values.

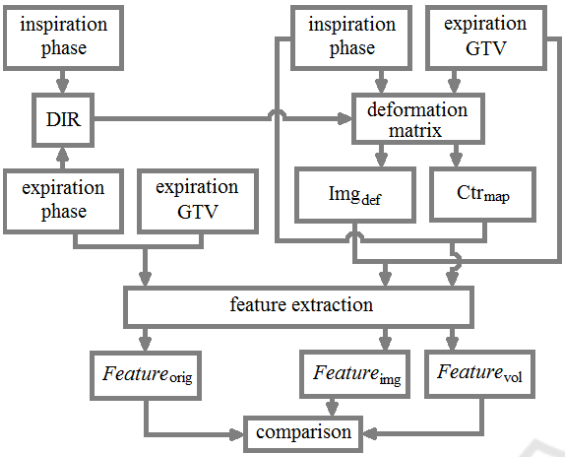

Figure 1: Analysis flow chart. Ctr_{map} = mapped contour; Img_{def} = deformed image; $Feature_{orig}$ = original feature, set as standard; $Feature_{img}$ = features extracted from the deformed image; $Feature_{vol}$ = features extracted from the mapped volume.

2.4 Feature Stability Analysis

Percentage differences between features after DIR and the standard ones were calculated as

$$\%Diff = 100 \times \left| \frac{Feature_{DIR} - Feature_{orig}}{Feature_{orig}} \right|, \quad (1)$$

where $Feature_{DIR}$ is the corresponding feature value with the DIR, either $Feature_{vol}$ or $Feature_{img}$. The percentage differences were averaged for each feature across all cases.

The concordance correlation coefficient (CCC) measures the reproducibility between two datasets (Lin, 1989). The CCC values are between 0 and ±1, with 0 being no correlation at all and ±1 being perfect concordance or perfect discordance. The CCC values were calculated for each feature between the standard, $Feature_{orig,}$ and one of the two sets after the DIR, either $Feature_{vol}$ or $Feature_{img}$.

The features with average variation greater than 50% or CCC lower than 0.5 were considered unstable, while the ones with average variation < 20% and CCC > 0.85 were categorized as acceptable. The rest were considered uncertain. Within the acceptable group the ones with variation < 10% and CCC > 0.9 were considered stable, and those with average variation < 5% and CCC > 0.95 were labeled as robust.

3 RESULTS

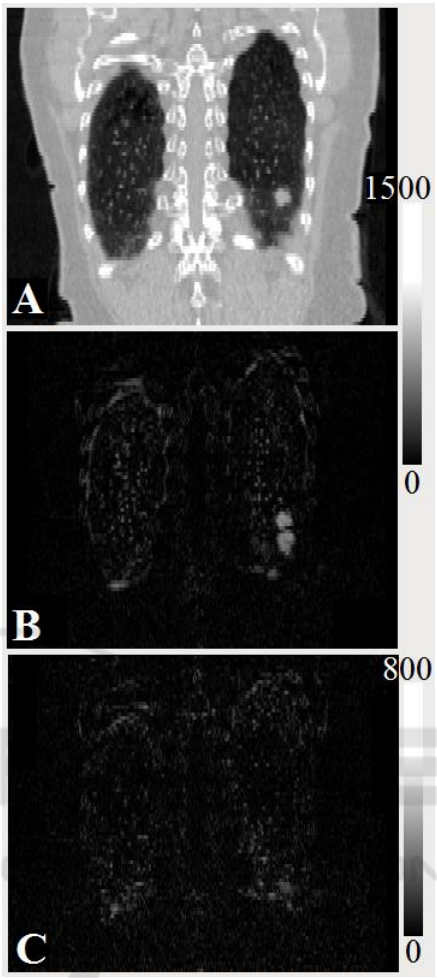

Figure 2: Example of image registration: (A) expiration phase, (B) absolute difference between expiration and inspiration, and (C) absolute difference between expiration and deformed and aligned inspiration-to-expiration.

Figure 2 shows an example of image registration. Notice different intensity scales between A, B (0~1500) and C (0~800). Without the scale adjustment, differences on panel C would not be visible. Overall, the differences between the mapped images and the expiration phase images were small.

Table 1 shows the overall percentage stable features for one of the two DIR approaches: mapped contour (Ctr_{map}) and Table 2 shows those for the other approach: deformed image (Img_{def}). Because the same contour was used in the mapped image feature calculation, the shape based features in this category are 100% stable/robust. Features from the categories of intensity, GLCM and FD are stable for both DIR approaches. Relatively more wavelet

features also were stable, while Laws features were the most unstable group for the filtered image features. The overall most unstable feature group was GLSZ.

Table 1: Percentage of features in various groups for mapped contour, Ctr_{map}.

	Unstable	Uncertain	Acceptable	Stable	Robust
Shape	30%	55%	15%	5%	0%
Intensity	5%	32%	63%	45%	16%
LoG	31%	21%	48%	38%	21%
Wavelet	23%	42%	35%	24%	12%
Laws	51%	28%	22%	9%	2%
GLCM	3%	30%	68%	40%	5%
RLM	18%	35%	47%	12%	0%
GLSZ	67%	17%	17%	17%	8%
NGTDM	45%	45%	9%	0%	0%
FD	0%	50%	50%	38%	13%

Table 2: Percentage of features in various groups for deformed image, Img_{def}.

	Unstable	Uncertain	Acceptable	Stable	Robust
Shape	0%	0%	100%	100%	100%
Intensity	3%	50%	47%	47%	45%
LoG	28%	36%	36%	16%	9%
Wavelet	2%	12%	86%	68%	39%
Laws	53%	32%	15%	7%	2%
GLCM	5%	38%	57%	28%	20%
RLM	18%	35%	47%	29%	6%
GLSZ	75%	8%	17%	17%	0%
NGTDM	64%	0%	36%	9%	0%
FD	0%	0%	100%	100%	75%

Table 3 shows some results of the detailed analysis of the filtered image features sub-categories for mapped contour. Table 4 shows those for deformed image. In the table, LoG_1 means the features in this sub-category were extracted with Gaussian kernel width of 1 mm, and so on. Similar analysis was performed on the Laws and wavelet features (not presented).

Table 5 lists the unstable features, excluding those from the filtered images (i.e. LoG, wavelet, Laws). For the filtered images, the numbers of unstable features were 339 for Img_{def} and 364 for Ctr_{map} out of 861. Among the LoG and Laws features, energy was the most unstable one in each sub-category.

Table 3: Percentage of LoG features in sub-categories for mapped contour.

	Unstable	Uncertain	Acceptable	Stable	Robust
LoG_0.5	0%	24%	76%	62%	29%
LoG_1	33%	19%	48%	38%	33%
LoG_1.5	43%	19%	38%	29%	5%
LoG_2	43%	19%	38%	19%	10%
LoG_2.5	33%	24%	43%	33%	33%
LoG_3	33%	19%	48%	48%	14%

Table 4: Percentage of LoG features in sub-categories for deformed image.

	Unstable	Uncertain	Acceptable	Stable	Robust
LoG_0.5	10%	14%	76%	52%	29%
LoG_1	33%	62%	5%	5%	5%
LoG_1.5	33%	57%	10%	5%	5%
LoG_2	38%	52%	10%	10%	5%
LoG_2.5	33%	19%	48%	10%	5%
LoG_3	19%	14%	67%	14%	5%

4 DISCUSSION

The feature variations observed after DIR can be the result of the deformation itself and/or DIR errors. Image deformation could change the voxel intensity relationships between neighboring voxels which in turn changes the feature values. In addition, the shape of the mapped volume is likely to differ from the original one, which changes the shape based feature values, such as the sphericity, compactness, convexity, etc. The DIR errors introduce further uncertainty. This study did not attempt to separate these two potential causes of variation.

To reduce the DIR errors, we used the 4DCT data, wherein the differences between the phases should be much smaller than differences arising from the use of dissimilar imaging modalities. However, due to the raw scan data being divided into multiple phase bins, the quantum noise in each phase is higher compared to the standard (3D) data set, which in turn may reduce the accuracy of DIR. As both DIR accuracy and feature values depend on image quality (Latifi et al., 2013a, Oliver et al., 2017), high quality images are essential for feature stability.

Since image feature stability depends on the registration algorithm accuracy (Cunliffe et al.,

2012), any DIR algorithm for applications in feature calculation should be evaluated first. This study was limited to one DIR algorithm.

Table 5: Unstable features. In the table, *Angle between short axis and xz plane; angle between short axis and free long axis; angle between free long axis and long axis through center of mass; **Vnorm = coarseness and volume normalized coarseness, 2 features; **V, Gnorm = texture strength, volume normalized and gray level normalized texture strength, 3 features.

Feature		Ctr_{map}	Img_{def}
Shape	Angle: short to xz*	X	
	Angle: short to long*	X	
	Angle: long to long COM*	X	
Intensity	skewness	X	X
	energy	X	
GLCM	correlation		X
	cluster shade	X	X
RLM	LGRE	X	X
	SRLGE	X	X
	LRLGE	X	X
GLSZ	SAE	X	X
	LAE		X
	LIE	X	X
	LISAE	X	X
	HISAE	X	X
	LIHAE	X	X
	HILAE	X	X
	IV	X	X
	HIE	X	X
NGTDM	coarseness, Vnorm**		X
	busyness	X	X
	texture strength, V, Gnorm**	X	X

The DIR-stable features varied significantly between clinical cases, or were sensitive to different conditions. For example, the intensity based entropy was robust with both DIR approaches (mean variation less than 5% in each case), but it varied up to 80% between the cases. Further clinical application studies may need to focus on those acceptable features when DIR is involved.

Many feature values are voxel size dependent (Shafiq-ul-Hassan et al., 2017). In this study, the comparison was performed between the two phases of the 4D same dataset, with no voxel size variation.

The definition of unstable features in this work was strict (mean variation > 50% or CCC < 0.5). Any feature falling into this category (listed in Table 5 for the unfiltered image features) should be really unstable and thus avoided in in the presence of DIR.

This study only used CT image data. However, due to the nature of DIR, the conclusions should be applicable to other imaging modalities as well.

5 CONCLUSIONS

We have investigated the impact of DIR on radiomic features after either contour propagation or image deformation. Deformable image registration modified radiomic features with either approach. The stability varied slightly with the way the DIR is applied for most of the feature categories. Many features varied significantly after DIR, and thus were categorized as unstable. Those features should be avoided in applications requiring DIR.

REFERENCES

Aerts, H. J. W. L., Velazquez, E. R., Leijenaar, R. T. H., Parmar, C., Grossmann, P., Carvalho, S., Bussink, J., Monshouwer, R., Haibe-Kains, B., Rietveld, D., Hoebers, F., Rietbergen, M. M., Leemans, C. R., Dekker, A., Quackenbush, J., Gillies, R. J. & Lambin, P. 2014. Decoding Tumour Phenotype By Noninvasive Imaging Using A Quantitative Radiomics Approach. *Nature Communications*, 5, 4006.

Amadasun, M. & King, R. 1989. Textural Features Corresponding To Textural Properties. *Ieee Transactions On Systems, Man, And Cybernetics*, 19, 1264-1274.

Antunes, J., Viswanath, S., Rusu, M., Valls, L., Hoimes, C., Avril, N. & Madabhushi, A. 2016. Radiomics Analysis On Flt-Pet/Mri For Characterization Of Early Treatment Response In Renal Cell Carcinoma: A Proof-Of-Concept Study. *Translational Oncology*, 9, 155-162.

Balagurunathan, Y., Gu, Y., Wang, H., Kumar, V., Grove, O., Hawkins, S., Kim, J., Goldgof, D. B., Hall, L. O., Gatenby, R. A. & Gillies, R. J. 2014. Reproducibility And Prognosis Of Quantitative Features Extracted From Ct Images. *Translational Oncology*, 7, 72-87.

Carles, M., Torres-Espallardo, I., Alberich-Bayarri, A., Olivas, C., Bello, P., Nestle, U. & Martí-Bonmatí, L. 2017. Evaluation Of Pet Texture Features With Heterogeneous Phantoms: Complementarity And Effect Of Motion And Segmentation Method. *Physics In Medicine And Biology*, 62, 652.

Chen, J. S., Huertas, A. & Medioni, G. 1987. Fast Convolution With Laplacian-Of-Gaussian Masks. *Ieee Transactions On Pattern Analysis And Machine Intelligence*, Pami-9, 584-590.

Chu, A., Sehgal, C. M. & Greenleaf, J. F. 1990. Use Of Gray Value Distribution Of Run Lengths For Texture Analysis. *Pattern Recognition Letters*, 11, 415-419.

Cunliffe, A., Armato Iii, S. G., Castillo, R., Pham, N., Guerrero, T. & Al-Hallaq, H. A. 2015. Lung Texture In Serial Thoracic Computed Tomography Scans: Correlation Of Radiomics-Based Features With Radiation Therapy Dose And Radiation Pneumonitis Development. *International Journal Of Radiation Oncology Biology Physics*, 91, 1048-1056.

Cunliffe, A. R., Al-Hallaq, H. A., Labby, Z. E., Pelizzari, C. A., Straus, C., Sensakovic, W. F., Ludwig, M., Armato, S. G. & Iii 2012. Lung Texture In Serial Thoracic Ct Scans: Assessment Of Change Introduced By Image Registration. *Med Phys*, 39, 4679-4690.

Fave, X., Zhang, L., Yang, J., Mackin, D., Balter, P., Gomez, D., Followill, D., Jones, A. K., Stingo, F. & Liao, Z. 2017. Delta-Radiomics Features For The Prediction Of Patient Outcomes In Non-Small Cell Lung Cancer. *Scientific Reports*, 7, 588.

Galavis, P. E., Hollensen, C., Jallow, N., Paliwal, B. & Jeraj, R. 2010. Variability Of Textural Features In Fdg Pet Images Due To Different Acquisition Modes And Reconstruction Parameters. *Acta Oncologica*, 49, 1012-1016.

Galloway, M. M. 1975. Texture Analysis Using Gray Level Run Lengths. *Computer Graphics And Image Processing*, 4, 172-179.

Gao, S., Zhang, L., Wang, H., Crevoisier, R. D., Kuban, D. D., Mohan, R. & Dong, L. 2006. A Deformable Image Registration Method To Handle Distended Rectums In Prostate Cancer Radiotherapy. *Med Phys*, 33, 3304-3312.

Haralick, R. M., Shanmugam, K. & Dinstein, I. H. 1973. Textural Features For Image Classification. *Systems, Man And Cybernetics, Ieee Transactions On*, Smc-3, 610-621.

Huang, T.-C., Hsiao, C.-Y., Chien, C.-R., Liang, J.-A., Shih, T.-C. & Zhang, G. 2013. Imrt Treatment Plans And Functional Planning With Functional Lung Imaging From 4d-Ct For Thoracic Cancer Patients. *Radiat Oncol*, 8, 3.

Janssens, G., Jacques, L., Orban De Xivry, J., Geets, X. & Macq, B. 2011. Diffeomorphic Registration Of Images With Variable Contrast Enhancement. *International Journal Of Biomedical Imaging*, 2011, Article Id 891585.

Jin, X. C., Ong, S. H. & Jayasooriah 1995. A Practical Method For Estimating Fractal Dimension. *Pattern Recognition Letters*, 16, 457-464.

Latifi, K., Huang, T.-C., Feygelman, V., Budzevich, M. M., Moros, E. G., Dilling, T. J., Stevens, C. W., Elmpt, W. V., Dekker, A. & Zhang, G. G. 2013a. Effects Of Quantum Noise In 4d-Ct On Deformable Image Registration And Derived Ventilation Data. *Phys Med Biol*, 58, 7661-7672.

Latifi, K., Zhang, G., Stawicki, M., Van Elmpt, W., Dekker, A. & Forster, K. 2013b. Validation Of Three Deformable Image Registration Algorithms For The Thorax. *J Appl Clin Med Phys*, 14, 19-30.

Liang, M. 2012. *3d Co-Occurrence Matrix Based Texture Analysis Applied To Cervical Cancer Screening.* Master, Uppsala University.

Lin, L. I. K. 1989. A Concordance Correlation Coefficient To Evaluate Reproducibility. *Biometrics*, 45, 255-268.

Nardone, V., Tini, P., Biondi, M., Sebaste, L., Vanzi, E., De Otto, G., Rubino, G., Carfagno, T., Battaglia, G. & Pastina, P. 2016. Prognostic Value Of Mr Imaging Texture Analysis In Brain Non-Small Cell Lung Cancer Oligo-Metastases Undergoing Stereotactic Irradiation. *Cureus*, 8.

Oliver, J. A., Budzevich, M., Hunt, D., Moros, E. G., Latifi, K., Dilling, T. J., Feygelman, V. & Zhang, G. 2017. Sensitivity Of Image Features To Noise In Conventional And Respiratory-Gated Pet/Ct Images Of Lung Cancer. *Technology In Cancer Research & Treatment*, 16, 595-608.

Oliver, J. A., Budzevich, M., Zhang, G. G., Dilling, T. J., Latifi, K. & Moros, E. G. 2015. Variability Of Image Features Computed From Conventional And Respiratory-Gated Pet/Ct Images Of Lung Cancer. *Translational Oncology*, 8, 524-534.

Sarkar, N. & Chaudhuri, B. B. 1992. An Efficient Approach To Estimate Fractal Dimension Of Textural Images. *Pattern Recognition*, 25, 1035-1041.

Shafiq-Ul-Hassan, M., Zhang, G. G., Latifi, K., Ullah, G., Hunt, D. C., Balagurunathan, Y., Abdalah, M. A., Schabath, M. B., Goldgof, D. G., Mackin, D., Court, L. E., Gillies, R. J. & Moros, E. G. 2017. Intrinsic Dependencies Of Ct Radiomic Features On Voxel Size And Number Of Gray Levels. *Medical Physics*, 44, 1050-1062.

Suzuki, M. T. & Yaginuma, Y. A Solid Texture Analysis Based On Three-Dimensional Convolution Kernels. 2007. 64910w-64910w-8.

Thibault, G., Fertil, B., Navarro, C., Pereira, S., Cau, P., Levy, N., Sequeira, J. & Mari, J.-L. Texture Indexes And Gray Level Size Zone Matrix: Application To Cell Nuclei Classification. 10th International Conference On Pattern Recognition And Information Processing, 2009 Minsk, Belarus. 140-145.

Uytterhoeven, G., Roose, D. & Bultheel, A. 1997. *Wavelet Transforms Using The Lifting Scheme*.

Wrangsjö, A., Pettersson, J. & Knutsson, H. 2005. Non-Rigid Registration Using Morphons. *In:* Kalviainen, H., Parkkinen, J. & Kaarna, A. (Eds.) *Image Analysis.* Springer Berlin Heidelberg.

Yip, S. S. F., Coroller, T. P., Sanford, N. N., Huynh, E., Mamon, H., Aerts, H. J. W. L. & Berbeco, R. I. 2016. Use Of Registration-Based Contour Propagation In Texture Analysis For Esophageal Cancer Pathologic Response Prediction. *Physics In Medicine And Biology*, 61, 906.